Eur. Phys. J. A **40**, 23–33 (2009)
DOI 10.1140/epja/i2008-10731-2

THE EUROPEAN PHYSICAL JOURNAL A

Regular Article – Experimental Physics

The dp → ppn reaction as a method to study neutron-proton charge-exchange amplitudes

D. Chiladze[1,2,3], J. Carbonell[4], S. Dymov[5,6], A. Dzyuba[7], V. Glagolev[8], M. Hartmann[2,3], A. Kacharava[2,3], I. Keshelashvili[1,9], A. Khoukaz[10], V. Komarov[5], P. Kulessa[11], A. Kulikov[5], N. Lomidze[1], G. Macharashvili[1,5], Y. Maeda[12], D. Mchedlishvili[1], T. Mersmann[10], S. Merzliakov[2,3,5], M. Mielke[10], S. Mikirtychyants[2,3,7], M. Nekipelov[2,3], M. Nioradze[1], H. Ohm[2,3], F. Rathmann[2,3], H. Ströher[2,3], M. Tabidze[1], S. Trusov[13], Yu. Uzikov[5], Yu. Valdau[7], and C. Wilkin[14,a]

[1] High Energy Physics Institute, Tbilisi State University, 0186 Tbilisi, Georgia
[2] Institut für Kernphysik, Forschungszentrum Jülich GmbH, 52425 Jülich, Germany
[3] Jülich Centre for Hadron Physics, 52425 Jülich, Germany
[4] Laboratoire de Physique Subatomique et de Cosmologie, 38026 Grenoble, France
[5] Laboratory of Nuclear Problems, JINR, 141980 Dubna, Russia
[6] Physikalisches Institut II, Universität Erlangen-Nürnberg, 91058 Erlangen, Germany
[7] High Energy Physics Department, Petersburg Nuclear Physics Institute, 188350 Gatchina, Russia
[8] Laboratory of High Energies, JINR, 141980 Dubna, Russia
[9] Department of Physics, University of Basel, Klingelbergstrasse 82, 4056 Basel, Switzerland
[10] Institut für Kernphysik, Universität Münster, 48149 Münster, Germany
[11] H. Niewodniczański Institute of Nuclear Physics PAN, 31342 Kraków, Poland
[12] Research Center for Nuclear Physics, Osaka University, Osaka Ibaraki, 567-0047, Japan
[13] Institut für Kern- und Hadronenphysik, Forschungszentrum Rossendorf, 01314 Dresden, Germany
[14] Physics and Astronomy Department, UCL, Gower Street, London, WC1E 6BT, UK

Received: 20 November 2008 / Revised: 21 January 2009
Published online: 5 March 2009 –
Communicated by T. Hennino

Abstract. The differential cross section and deuteron analysing powers of the $\vec{d}p \to \{pp\}n$ charge-exchange reaction have been measured with the ANKE spectrometer at the COSY storage ring. Using a deuteron beam of energy 1170 MeV, data were obtained for small momentum transfers to a $\{pp\}$ system with low excitation energy. A good quantitative understanding of all the measured observables is provided by the impulse approximation using known neutron-proton amplitudes. The proof of principle achieved here for the method suggests that measurements at higher energies will provide useful information in regions where the existing np database is far less reliable.

PACS. 13.75.-n Hadron-induced low- and intermediate-energy reactions and scattering (energy ≤ 10 GeV) – 25.45.De Elastic and inelastic scattering – 25.45.Kk Charge-exchange reactions

1 Introduction

An understanding of the NN interaction is fundamental to the whole of nuclear and hadronic physics. The database on proton-proton elastic scattering is enormous and the wealth of spin-dependent quantities measured has allowed the extraction of NN phase shifts in the isospin $I = 1$ channel up to a beam energy of at least 2 GeV [1]. The situation is far less advanced for the isoscalar channel where the much poorer neutron-proton data only permit the $I = 0$ phase shifts to be evaluated up to at most 1.3 GeV but with significant ambiguity above about 800 MeV [1]. The data on which such an analysis is based come from many facilities and it is incumbent on a laboratory that can make a significant contribution to the communal effort to do so.

It has recently been argued that, even without measuring triple-spin observables, a direct amplitude reconstruction of the neutron-proton backward scattering amplitudes might be possible with few ambiguities provided that experiments on the deuteron are included [2]. This work studied in detail the ratio of the forward charge-exchange cross-section of a neutron on a deuterium target

[a] e-mail: cw@hep.ucl.ac.uk

to that on a hydrogen target,

$$R_{np}(0) = \frac{\mathrm{d}\sigma(nd \to pnn)/\mathrm{d}t}{\mathrm{d}\sigma(np \to pn)/\mathrm{d}t}\,, \qquad (1.1)$$

where t is the four-momentum transfer between the initial neutron and final proton.

Due to the Pauli principle, when the two final neutrons are in a relative S-wave their spins must be antiparallel and the system is in the $^1S_0$ state. Under such circumstances the $nd \to p\{nn\}$ reaction involves a spin flip from the $S = 1$ of the deuteron to the $S = 0$ of the dineutron and hence it is dependent on the np spin-isospin-flip amplitudes. If the data are summed over all excitation energies of the nn system, then the Dean closure sum rule allows one to deduce from R_{np} the fraction of spin-dependence in the pn charge-exchange amplitudes [3]. Such measurements have now been carried out up to 2 GeV [4].

However, Bugg and Wilkin [5] have shown that much more information on the np charge-exchange amplitudes can be extracted by using a polarised deuteron beam or target and studying the charge-symmetric $\vec{d}p \to \{pp\}n$ reaction. To achieve the full benefit, the excitation energy E_{pp} in the final pp system must be kept low. Experiments from a few hundred MeV up to 2 GeV [6,7] have generally borne out the theoretical predictions and have therefore given hope that such experiments might provide valuable data on the amplitudes in the small momentum transfer region.

The ANKE Collaboration is embarking on a systematic programme to measure the differential cross-section and analysing powers of the $\vec{d}p \to \{pp\}n$ reaction up to the maximum energy of the COSY accelerator of 1.15 GeV per nucleon, with the aim of deducing information on the np amplitudes [8]. Higher energies per nucleon will be achieved through the use of a deuterium target. Spin correlations will also be studied with a polarised beam and target [9]. However, for these to be valid objectives, the methodology has to be checked in a region where the neutron-proton amplitudes are reasonably well known.

The first evaluation of the analysing powers of the $\vec{d}p \to \{pp\}n$ reaction at $T_d = 1170$ MeV reported in ref. [10] largely agrees with theoretical expectations. It is the purpose of the present work to refine this analysis and to establish also the cross-section normalisation. In this way the magnitudes of individual charge-exchange amplitudes could be tested and not merely their ratios.

Although the impulse approximation description of the $dp \to \{pp\}n$ reaction is to be found in several papers [5, 11], a brief resumé is presented in sect. 2 for the ideal case where the final pp system is in a pure $^1S_0$ state. The general layout and capabilities of the ANKE facility are described in sect. 3. The normalisation of the charge-exchange cross-sections is achieved relative to the quasi-free $dp \to p_{\mathrm{sp}}d\pi^0$ reaction; the detection of a spectator proton in coincidence with the deuteron, produced *via* $np \to d\pi^0$, closely matches the acceptance for the two charge-exchange protons. These measurements are described in sect. 4. The luminosity obtained by comparing the results with those in the literature allows the unpolarised $dp \to \{pp\}n$ differential cross-section to be determined, as shown in sect. 5. Some check on the luminosity could be provided through the study of elastic deuteron-proton scattering, though there are larger uncertainties in the relevant World database.

In order that the deuteron analysing powers can be measured, the value of the polarisation has to be established for each of the modes of the ion source used in the preparation of the beam. By using the charge-exchange data themselves, it has proved possible to reduce the statistical error bars residing in the earlier analysis [10,12] and this is explained in sect. 6. The evaluation of the $\vec{d}p \to \{pp\}n$ analysing powers as a function of the momentum transfer in two bins of E_{pp} is the subject treated in sect. 7.

Since both the cross-section and two tensor analysing powers at 585 MeV per nucleon agree with theoretical predictions based upon reliable neutron-proton phase-shift analysis, this gives us confidence that the methods used here can be extended to higher energies where much less is known about the np elastic amplitudes. The possibilities of such work are discussed in sect. 8.

2 Impulse approximation dynamics

Bugg and Wilkin studied the cross-section and deuteron analysing powers of the $\vec{d}p \to \{pp\}n$ reaction within the impulse approximation [5] and their results were refined through the use of more realistic low-energy nucleon-nucleon interactions in ref. [11]. In this approach it is assumed that the driving mechanism is a quasi-free (p,n) charge exchange on the neutron in the deuteron. The resulting matrix element is then proportional to that for $pn \to np$ times a form factor that depends upon the deuteron and pp wave functions and the momentum transfer $\boldsymbol{q}$. There is a strong interplay between the spin-dependence of the np amplitudes and the polarisation of the initial deuteron and this leads to very significant deuteron tensor analysing powers. However, it is crucial to note that these analysing powers tend to have opposite signs for spin-singlet and spin-triplet pp final states [5]. As a consequence, the sizes of the resulting effects will depend strongly on the limits placed upon the pp excitation energy in order to isolate the $^1S_0$ state. We here merely present explicitly the formalism for a pure S-wave state while recognising that the detailed comparison of data with theory requires a much more thorough numerical evaluation of the full model [11].

The charge-exchange amplitude of the elementary $np \to pn$ scattering may be written in terms of five scalar amplitudes in the cm system as

$$f_{np} = \alpha(q) + i\gamma(q)(\boldsymbol{\sigma}_1 + \boldsymbol{\sigma}_2)\cdot\boldsymbol{n} + \beta(q)(\boldsymbol{\sigma}_1\cdot\mathbf{n})(\boldsymbol{\sigma}_2\cdot\boldsymbol{n}) + \delta(q)(\boldsymbol{\sigma}_1\cdot\boldsymbol{m})(\boldsymbol{\sigma}_2\cdot\boldsymbol{m}) + \varepsilon(q)(\boldsymbol{\sigma}_1\cdot\boldsymbol{l})(\boldsymbol{\sigma}_2\cdot\boldsymbol{l}), \quad (2.1)$$

where $\boldsymbol{\sigma}_1$ is the Pauli matrix between the initial neutron and final proton, and the reverse for $\boldsymbol{\sigma}_2$. The relationship between these and the standard elastic amplitudes

is explained in some detail in ref. [2]. Here α is the spin-independent amplitude between the initial neutron and final proton, γ is a spin-orbit contribution, and β, δ, and ε are the spin-spin terms. The one-pion-exchange pole is contained purely in the δ amplitude and this gives rise to its very rapid variation with momentum transfer, which influences very strongly the deuteron charge-exchange observables.

The orthogonal unit vectors are defined in terms of the initial neutron ($\boldsymbol{K}$) and final proton ($\boldsymbol{K'}$) momenta;

$$\boldsymbol{n} = \frac{\boldsymbol{K} \times \boldsymbol{K'}}{|\boldsymbol{K} \times \boldsymbol{K'}|}, \qquad \boldsymbol{m} = \frac{\boldsymbol{K'} - \boldsymbol{K}}{|\boldsymbol{K'} - \boldsymbol{K}|}, \qquad \boldsymbol{l} = \frac{\boldsymbol{K'} + \boldsymbol{K}}{|\boldsymbol{K'} + \boldsymbol{K}|}. \tag{2.2}$$

The amplitudes are normalised such that the elementary $np \to pn$ differential cross-section has the form

$$\left(\frac{\mathrm{d}\sigma}{\mathrm{d}t}\right)_{np\to pn} = |\alpha(q)|^2 + |\beta(q)|^2 + 2|\gamma(q)|^2 + |\delta(q)|^2 + |\varepsilon(q)|^2 . \tag{2.3}$$

In impulse approximation the deuteron charge-exchange amplitude to the ${}^1S_0$ state depends only upon the spin-dependent parts of f_{np} [5]. The form factor describing the transition from a deuteron to a ${}^1S_0$-state of the final pp pair contains two terms

$$\begin{aligned} S^+\left(k, \frac{1}{2}q\right) &= F_S\left(k, \frac{1}{2}q\right) + \sqrt{2}F_D\left(k, \frac{1}{2}q\right), \\ S^-\left(k, \frac{1}{2}q\right) &= F_S\left(k, \frac{1}{2}q\right) - F_D\left(k, \frac{1}{2}q\right) \Big/ \sqrt{2}. \end{aligned} \tag{2.4}$$

Here $\boldsymbol{q}$ is the three-momentum transfer between the proton and neutron which, for small E_{pp}, is related to the four-momentum transfer by $t = -\boldsymbol{q}^2$.

The S^+ and S^- denote the longitudinal ($\lambda = 0$) and transverse ($\lambda = \pm 1$) form factors, where λ is the spin projection of the deuteron. The matrix elements F_S and F_D can be expressed in terms of the S- and D-state components of the deuteron wave function $u(r)$ and $w(r)$ as

$$F_S\left(k, \frac{1}{2}q\right) = \langle \psi_k^{(-)} | j_0\left(\frac{1}{2}qr\right) | u \rangle, \tag{2.5}$$

$$F_D\left(k, \frac{1}{2}q\right) = \langle \psi_k^{(-)} | j_2\left(\frac{1}{2}qr\right) | w \rangle. \tag{2.6}$$

The influence of the strong pp final-state interaction in the ${}^1S_0$ channel is automatically included through the use of the scattering wave function $\psi_k^{(-)}(r)$ that is obtained from the solution of the Schrödinger equation where both the strong and Coulomb potentials are included [11].

The pp relative momentum, $\boldsymbol{k}$, corresponds to an excitation energy $E_{pp} = \boldsymbol{k}^2/m$, where m is the proton mass. We denote the ratio of the transition form factors by

$$\mathcal{R} = S^+\left(k, \frac{1}{2}q\right) \Big/ S^-\left(k, \frac{1}{2}q\right) \tag{2.7}$$

and the combination of modulus squares of amplitudes by

$$I = |\beta(q)|^2 + |\gamma(q)|^2 + |\varepsilon(q)|^2 + |\delta(q)|^2 |\mathcal{R}|^2. \tag{2.8}$$

Impulse approximation applied to $dp \to \{pp\}_{^1S_0} n$ then leads to the following predictions for the differential cross-section and deuteron spherical analysing powers [5,11]:

$$\begin{aligned} \frac{\mathrm{d}^4\sigma}{\mathrm{d}t\,\mathrm{d}^3k} &= I\left[S^-\left(k, \frac{1}{2}q\right)\right]^2 \Big/ 3, \\ I\,it_{11} &= 0, \\ I\,t_{20} &= \left[|\beta(q)|^2 + |\delta(q)|^2|\mathcal{R}|^2 - 2|\varepsilon(q)|^2 + |\gamma(q)|^2\right]/\sqrt{2}, \\ I\,t_{22} &= \sqrt{3}\left[|\beta(q)|^2 - |\delta(q)|^2|\mathcal{R}|^2 + |\gamma(q)|^2\right]/2. \end{aligned} \tag{2.9}$$

In this ${}^1S_0$ limit, a measurement of the differential cross-section, t_{20}, and t_{22} would allow one to extract values of $|\beta(q)|^2 + |\gamma(q)|^2$, $|\delta(q)|^2$, and $|\varepsilon(q)|^2$ for small values of the momentum transfer $\boldsymbol{q}$ between the initial proton and final neutron. However, even if a sharp cut of 1 MeV is placed upon E_{pp}, there still remain small contributions from proton-proton P-waves that dilute the analysing power signal. Such effects must be included in any analysis aimed at providing quantitative information on the neutron-proton amplitudes [11].

One way of reducing the dilution of the tensor analysing powers by the P-waves is by imposing a cut on the angle θ_{qk} between the momentum transfer $\boldsymbol{q}$ and the relative momentum $\boldsymbol{k}$ between the two protons. When these two vectors are perpendicular, impulse approximation does not allow the excitation of odd partial waves in the pp system [5] and this is in agreement with available experimental data [7].

In terms of the charge-exchange amplitudes, the Dean sum rule [3] for the ratio of the forward $nd \to pnn$ to $np \to pn$ cross-sections of eq. (1.1) becomes

$$R_{np}(0) = \frac{2}{3}\left[\frac{2|\beta(0)|^2 + |\varepsilon(0)|^2}{|\alpha(0)|^2 + 2|\beta(0)|^2 + |\varepsilon(0)|^2}\right]. \tag{2.10}$$

The same result should, of course, hold for $dp \to ppn$, which is the reaction studied at ANKE.

3 The experimental facility

The COSY COoler SYnchrotron of the Forschungszentrum Jülich is capable of accelerating and storing protons and deuterons with momenta up to 3.7 GeV/c [13]. The ANKE magnetic spectrometer of fig. 1 used for the deuteron charge-exchange study is located at an internal target position that forms a chicane in the storage ring. Although ANKE contains several detection possibilities [14], only those of the Forward Detector (FD) system were used to measure the two fast protons from the $dp \to \{pp\}n$ charge exchange [10], as well as the products associated with the calibration reactions. The FD consists of multiwire chambers for track reconstruction and three layers of a scintillation hodoscope that permit time-of-flight and energy loss determinations [15]. The measurements were carried out using a polarised deuteron beam and a hydrogen cluster jet target [16]. The main trigger used in the experiment consisted of a coincidence of different layers in the hodoscope of the FD.

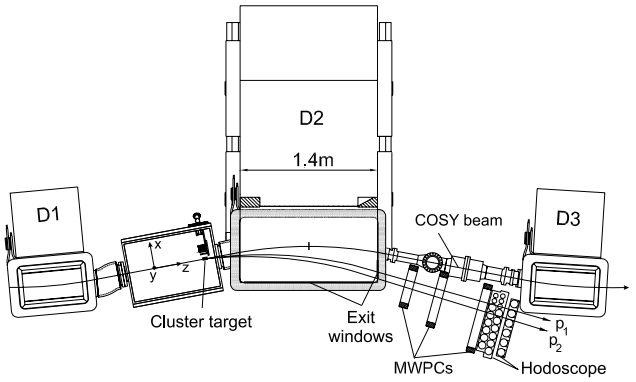

Fig. 1. Top view of the ANKE experimental set-up, showing the positions of the three dipole magnets D1, D2, and D3. The hydrogen cluster jet injects target material vertically downwards. The Forward Detector (FD) consists of three MWPCs and a hodoscope composed of three layers of scintillation counters.

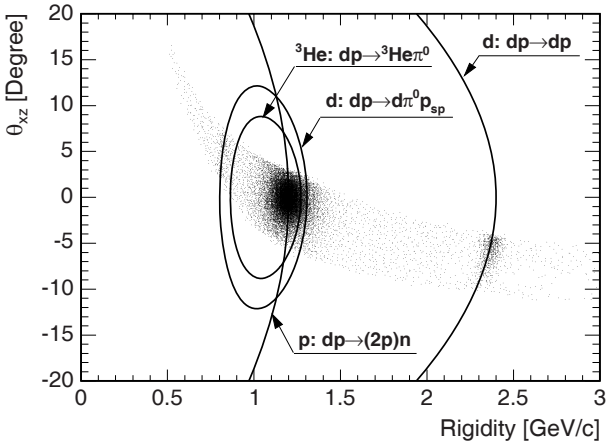

Fig. 2. ANKE experimental acceptance for four nuclear reactions of interest at a deuteron momentum of $p_d = 2400\,\mathrm{MeV}/c$.

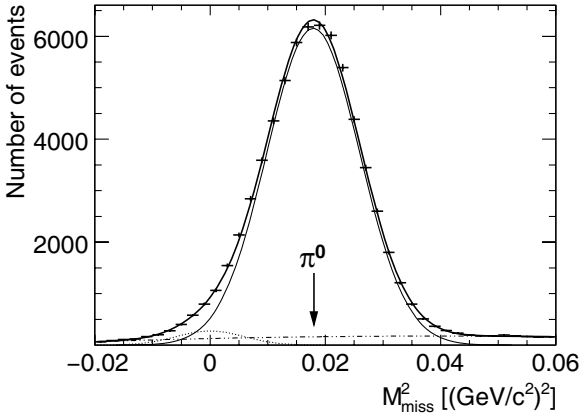

Fig. 3. Missing-mass–squared distribution for the $dp \to p_{\mathrm{sp}}dX$ reaction for the fast deuteron branch of the kinematics. A fit to the data with a Gaussian and a constant background is indicated. Some of the event excess for $M^2_{\mathrm{miss}} \approx 0$ might be associated with the quasi-free $np \to d\gamma$ reaction, which is included in the fit as the dotted curve.

Figure 2 shows the experimental acceptance of ANKE for single particles at $T_d = 1170\,\mathrm{MeV}$ in terms of the laboratory production angle in the horizontal plane and the magnetic rigidity. The kinematical loci for various nuclear reactions are also illustrated. In addition to the protons from the deuteron charge exchange $dp \to \{pp\}n$, of particular interest are the deuterons produced in the quasi-free $dp \to p_{\mathrm{sp}}d\pi^0$ reaction with a fast spectator proton, p_{sp}. It is important to note that these spectators, as well as those from the deuteron breakup, $dp \to p_{\mathrm{sp}}pn$, have essentially identical kinematics to those of the charge-exchange protons. As a consequence, the $(d, 2p)$ reaction can only be distinguished from other processes yielding a proton spectator by carrying out coincidence measurements. Deuterons elastically scattered at small angles are well separated from the other particles in fig. 2.

4 Luminosity measurements

4.1 Quasi-free pion production

Both the fast deuteron and the spectator proton, p_{sp}, from the $dp \to p_{\mathrm{sp}}d\pi^0$ reaction have momenta that are very similar to those of the two protons in the $dp \to \{pp\}n$ reaction. Any error in the estimation of the two-particle acceptance will therefore tend to cancel between the two reactions. Interpreting the data in terms of quasi-free pion production, $np \to d\pi^0$, the counting rates for the $dp \to p_{\mathrm{sp}}d\pi^0$ reaction will allow a useful evaluation of the luminosity to be made.

The first step in extracting quasi-free $dp \to p_{\mathrm{sp}}d\pi^0$ candidates from the data is to choose two-track events using the MWPC information. The momentum vectors were determined from the magnetic-field map of the spectrometer, assuming a point-like source placed in the centre of the beam-target interaction region. The potential $dp \to p_{\mathrm{sp}}dX$ events can be clearly identified by studying the correlation of the measured time difference between the two hits on the hodoscope with that calculated on the basis of the two momenta and the distances from the target [12]. In order to ensure that the kinematics are similar to the two protons from the charge exchange at low E_{pp}, a cut is made on the difference between the momenta of the assumed proton and deuteron of $\Delta p < 175\,\mathrm{MeV}/c$. An analogous cut was placed upon the simulation of the acceptance.

The $dp \to p_{\mathrm{sp}}d\pi^0$ identification is completed by studying the missing mass of the reaction with respect to the final dp pair, as shown in fig. 3. The Δp cut means that only events corresponding to the forward deuteron branch are presented here. As is seen from fig. 2, these ones have similar acceptance to that of the $dp \to \{pp\}n$ reaction. The data show a very prominent π^0 peak though there is evidence for background on the low M^2_{miss} side, some of which might arise from the quasi-free $np \to d\gamma$ reaction.

To confirm the spectator hypothesis, a Monte Carlo simulation has been performed within PLUTO [17] using the Fermi momentum distribution evaluated from the

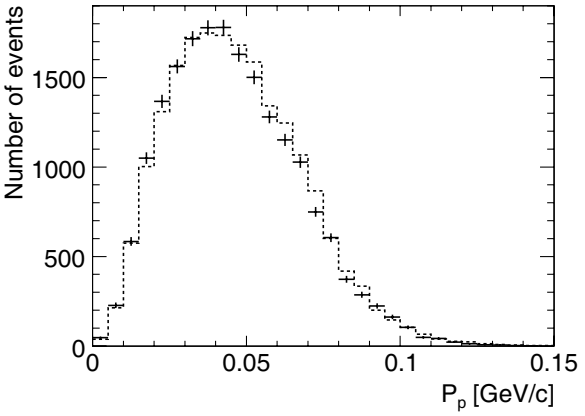

Fig. 4. Momentum distribution of the fast proton from the $dp \to p_{\rm sp}d\pi^0$ reaction transformed into the rest frame of the initial deuteron (histogram). The simulation (crosses) uses the Fermi momentum distribution obtained from the Paris deuteron wave function [18]. Only data with $p_{\rm sp} < 60\,{\rm MeV}/c$ were used in the evaluation of the luminosity.

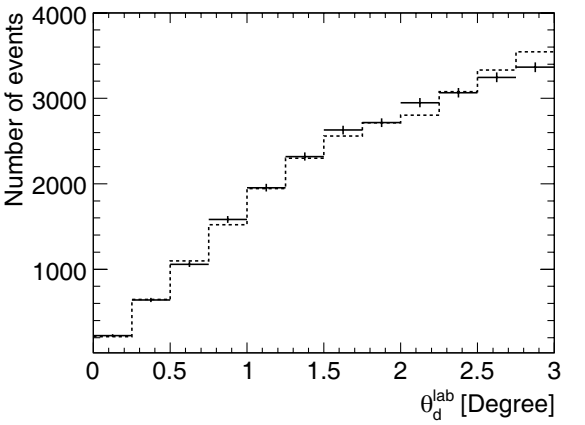

Fig. 5. Corrected numbers of counts of quasi-free $np \to d\pi^0$ events in 0.25° bins (crosses). The histogram represents the prediction of the $pp \to d\pi^+$ differential cross-section taken from the SAID program [19]. After taking an isospin factor of two into account, scaling the simulation to agree with the experimental points allows the luminosity to be evaluated.

Paris deuteron wave function [18]. As is clear from fig. 4, the data are completely consistent with quasi-free production on the neutron leading to a spectator proton. However, in order to reduce further possible contributions from multiple scattering and other mechanisms, only events with $p_{\rm sp} < 60\,{\rm MeV}/c$ were retained for the luminosity evaluation. The numbers of events were then corrected for acceptance and data acquisition efficiency *etc.* and presented in 0.25° bins of deuteron laboratory angle in fig. 5.

Isospin invariance requires that the differential cross-section for $np \to d\pi^0$ should be half that of the $pp \to d\pi^+$ reaction, for which there are many measurements and an extensive data compilation by the SAID group [19]. Predictions of the SAID program reproduce well the shape of the data in fig. 5 and, after scaling this to agree with our experimental points, the luminosity can be deduced. It is

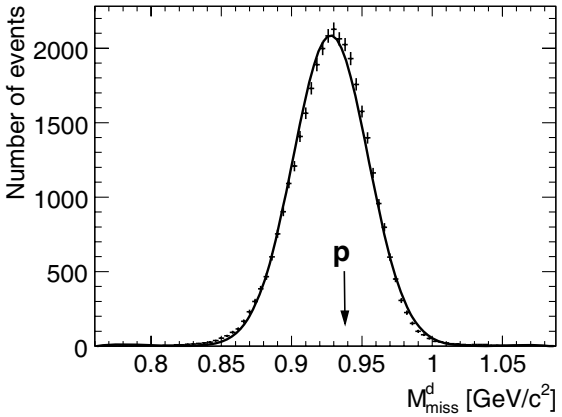

Fig. 6. The missing mass with respect of the observed deuterons for events that are close to the expected dp elastic locus in fig. 2. There is little or no background under the proton peak, which has a width of $\sigma = 27\,{\rm MeV}/c^2$.

of course possible that there could be small isospin violations between π^0 and π^+ production which may introduce uncertainties in the luminosity on the very few per cent level.

The luminosity determined in this way corresponds to that of the unpolarised mode. However, the orbit of the deuterons inside COSY should be independent of the polarisation mode of the ion source and so the relative luminosity for the other modes can be evaluated using the information provided by the beam-current transformer (BCT) [12].

4.2 Deuteron-proton elastic scattering

An alternative way of determining the luminosity required to evaluate the charge-exchange cross-section would be through the measurement of the deuteron-proton elastic scattering using data from the unpolarised spin mode. Due to its very high cross-section, the fast deuterons from this process are clearly seen in the angle-momentum plot of fig. 2 for laboratory polar angles from 5° to 10°. Since the locus of this reaction is well separated from those of the others, it is to be expected that the background should be very small. The justification for this is to be found in fig. 6 where, after selecting events from a broad region around the (p, θ_{xz}) locus, the missing mass with respect to the deuteron shows a proton peak with negligible background. As discussed below, the very different populations along the locus is merely a reflection of the rapid variation of the differential cross-section with angle.

Having identified good dp elastic scattering events, their numbers were corrected for the MWPC efficiency. For this purpose, two-dimensional efficiency maps were created for each plane and the tracks weighted using these maps. The events were grouped into laboratory polar angular bins of width 0.5° in order to plot the angular distribution. The numbers in each bin were adjusted by the prescaling factor using the correction of the DAQ efficiency. The resulting differential cross-section is plotted

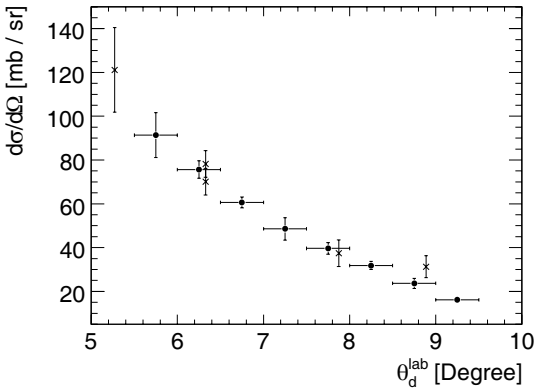

Fig. 7. Laboratory differential cross-section for small-angle dp elastic scattering in 0.5° bins (circles) are compared to the $pd \to pd$ values reported in ref. [20] and transformed to the proton rest frame (crosses). By scaling our data to agree with these values, an estimate of the luminosity could be made. Only data in the range $5.5° < \theta_d^{\rm lab} < 9.5°$ were used for this purpose.

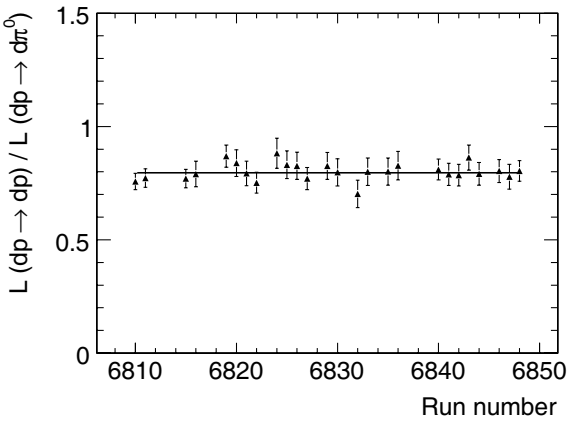

Fig. 8. Ratio of the luminosity determined from small-angle deuteron-proton elastic scattering and quasi-free $np \to d\pi^0$ pion production *versus* the individual run number.

as a function of the deuteron laboratory angle in fig. 7, using the normalisation discussed below.

Very close to our energy ($T_d/2 = 585\,\text{MeV}$) elastic proton-deuteron scattering was measured at 582 MeV using carbon and deuterated polyethylene targets together with counter telescopes [20]. The differential cross-sections were then obtained from a $CD_2 - C$ subtraction. The resulting values, transformed to the proton rest frame, are also shown in fig. 7. Although the absolute normalisation was established well using the carbon activation technique, it should be noted that a test measurement at one angle, where a magnetic spectrometer was used to suppress background from breakup protons, led to a cross-section that was 10% lower, though with a significant statistical error. There is therefore the possibility that these data include some contamination from non-elastic events. Despite this uncertainty, the comparison of the two data sets allows a value of the luminosity to be deduced for our experiment. To avoid regions of strong azimuthal variation in the ANKE acceptance, only the range $5.5° < \theta_d^{\rm lab} < 9.5°$ was considered for this evaluation.

The only other available data close to our momentum ($p_d = 2.4\,\text{GeV}/c$) come from a measurement of deuteron-proton elastic scattering in a hydrogen bubble chamber experiment at ten momenta between 2.0 and $3.7\,\text{GeV}/c$ [21]. Although numerical values are not available, the results show a smooth variation with momentum when plotted as a function of the momentum transfer t. Interpolating these results to 582 MeV, the data seem to be consistent with those of ref. [20], though the variation of the cross-section with t is extremely strong.

4.3 Comparison of the luminosity determinations

Having determined the luminosity independently of the basis of the $dp \to dp$ and quasi-free $np \to d\pi^0$ measurements, the results are compared in fig. 8 for all the individual "good" runs. The luminosity ratio is consistent with being constant,

$$\mathcal{L}(dp \to dp)/\mathcal{L}(np \to d\pi^0) = 0.80 \pm 0.01, \qquad (4.1)$$

where the error is purely statistical. The smallness of the fluctuations in fig. 8 implies that the two methods are sensitive to the same quantity, though with a different overall normalisation. Of the 20% discrepancy, about 5% can be accounted for by the shadowing correction [22], which reduces slightly the quasi-free cross-sections on the deuteron compared to their free values. To a first approximation the deuteron charge exchange would be subject to a rather similar shadowing correction. Some of the residual difference might be due to inelastic events in the published data [20].

Apart from the shortages in the World data set on $dp \to dp$ compared to $pp \to d\pi^+$, it should be noted that the elastic deuteron-proton differential cross-section varies very rapidly with angle. A shift of a mere 0.1° in the deuteron laboratory angle induces a 5% change in the cross-section. This is to be compared to the absolute precision in the angle determination in ANKE, which is $\approx 0.2°$. For these reasons much more confidence can be ascribed to the quasi-free $np \to d\pi^0$ method to determine the luminosity, which we believe to be accurate to better than about 4%, based upon the study of the errors quoted in $pp \to \pi^+ d$ measurements in this energy region [19]. The resulting integrated luminosity for the unpolarised mode was $\mathcal{L} = (12.5 \pm 0.5)\,\text{nb}^{-1}$.

5 Deuteron charge-exchange cross-section

The deuteron charge exchange on hydrogen, $dp \to \{pp\}n$ is defined to be the reaction where the diproton emerges with low excitation energy E_{pp}. When this takes place with small momentum transfer, the two fast protons are emitted in a narrow forward cone with momenta around half that of the deuteron beam. As described fully in ref. [10], such coincident pairs can be clearly identified using information from the FD system in much the same

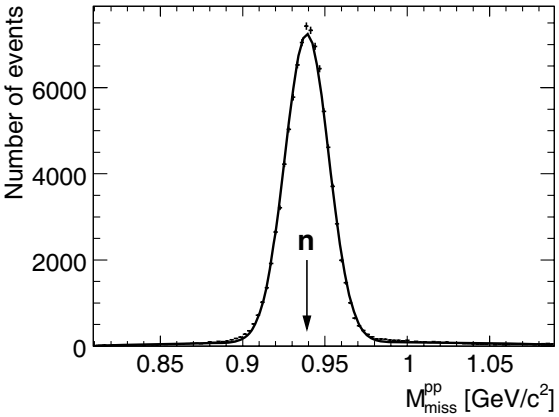

Fig. 9. Missing-mass distribution for proton pairs selected by the TOF criterion described in the text. A fit to the data in terms of a Gaussian plus a smoothly varying background shows the latter to be at about the 2% level. The central value agrees with the neutron mass to within 0.1%. Events falling within $\pm 2.5\sigma$ of the peak position were retained in the analysis.

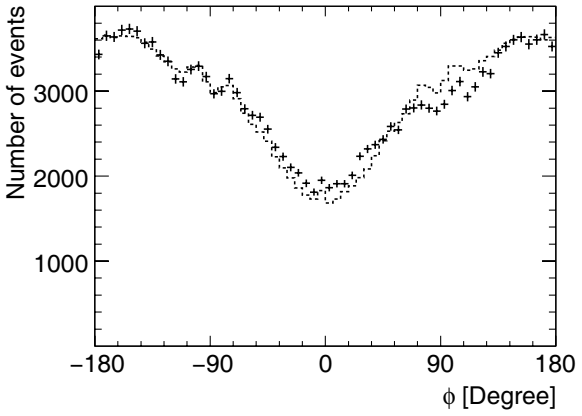

Fig. 10. Distribution of $dp \to \{pp\}n$ events in the azimuthal angle ϕ obtained with an unpolarised beam for $E_{pp} < 3\,\mathrm{MeV}$ (dashed line) compared to a simulation of expected events (crosses).

way as for the $dp \to p_{\mathrm{sp}}d\pi^0$ reaction of sect. 4.1. Having measured the momenta of two charged particles, their times of flight from the target to the hodoscope were calculated assuming that these particles were indeed protons. The difference between these two times of flight was compared with the measured time difference for those events where the particles hit different counters in the hodoscope. This selection, which discarded about 20% of the events, eliminated almost all the physics background, for example, from dp pairs associated with π^0 production. The resulting missing-mass distribution for identified ppX events shows a clean neutron peak in fig. 9 at $M_X = (940.4 \pm 0.2)\,\mathrm{MeV}/c^2$ with a width of $\sigma = 13\,\mathrm{MeV}/c^2$, sitting on a slowly varying 2% background.

Only at small momentum transfer and small pp excitation energy is the ANKE geometric acceptance even approximately isotropic. Unlike the case of $dp \to p_{\mathrm{sp}}d\pi^0$ used for the luminosity determination, one clearly cannot limit the data selection to this small region of phase space. Figure 10 shows the distribution of unpolarised charge-exchange events for $E_{pp} < 3\,\mathrm{MeV}$ in terms of the azimuthal angle of the diproton ϕ measured with respect to the COSY plane. This variable is of critical importance in the separation of the deuteron analysing powers for the $\vec{d}p \to \{pp\}n$ reaction and so it is necessary to have a reasonable understanding of its behaviour within a reliable GEANT simulation. As can be seen from fig. 10, this has been successfully achieved.

Since the counting rate varies rapidly with both E_{pp} and q, the acceptance was estimated by inserting the predictions of the impulse approximation model into the Monte Carlo simulation in a two-dimensional grid. Having then corrected the numbers of events for acceptance and DAQ and other efficiencies, the cross-sections found on the basis of the quasi-free $np \to d\pi^0$ luminosity were put in (E_{pp}, q) bins. The results obtained by summing these data over the interval in momentum transfer $0 < q < 100\,\mathrm{MeV}/c$ are presented as a function of E_{pp} in fig. 11.

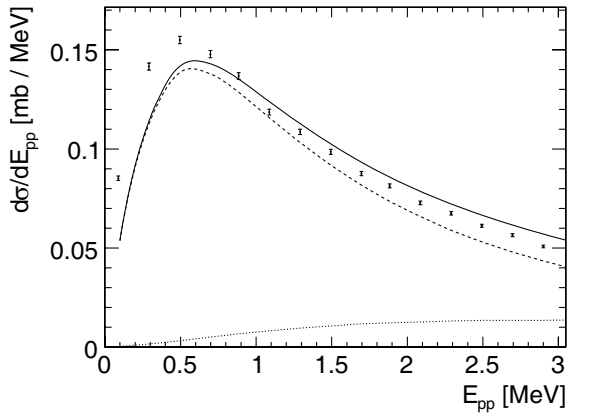

Fig. 11. Differential cross-section for unpolarised $dp \to \{pp\}n$ integrated over momentum transfer $q < 100\,\mathrm{MeV}/c$ as a function of the excitation energy E_{pp}. Only statistical errors are shown. The impulse approximation predictions [11] are shown separately for the $^1S_0$ (dashed curve) and higher waves (dotted curve) as well as their sum (solid curve).

The impulse approximation estimates shown in fig. 11 were obtained using a realistic pp potential that included the Coulomb force [11]. The neutron-proton charge-exchange amplitudes used here and for the later figures were taken from the current SAID solution [1]. The experimental results are reasonably well described even in absolute magnitude, although the model predictions are pushed to slightly higher values of E_{pp} than the data. This is probably due to event migration, since the resolution in E_{pp} is estimated to be about 300 keV. By summing events up to 3 MeV, where the prediction is smoothly varying, the effect of this on the differential cross-section is at most at the few per cent level.

However, it is important to note that, even for excitation energies as low as 3 MeV, there are significant contributions from higher partial waves. These arise preferentially for this reaction because even a small momentum kick to the neutron when it undergoes a charge ex-

Table 1. The configurations of the polarised deuteron ion source, showing the ideal values of the vector and tensor polarisations and their measurement using the EDDA polarimeter at a beam energy of $T_d = 270\,\mathrm{MeV}$ [24]. The standardised values of P_{zz} obtained on the basis of all the deuteron charge-exchange data are given in the final column. However, it should be noted that mode 0 was indeed completely unpolarised and the statistical error quoted here is merely to show that the charge-exchange data were completely consistent with that.

Mode n	P_z^{Ideal}	P_z^{EDDA}	P_{zz}^{Ideal}	P_{zz}^{EDDA}	P_{zz}^{Sta}
0	0	0	0	0	-0.006 ± 0.016
1	$-2/3$	-0.499 ± 0.021	0	0.057 ± 0.051	0.040 ± 0.016
2	$+1/3$	0.290 ± 0.023	$+1$	0.594 ± 0.050	0.658 ± 0.032
3	$-1/3$	-0.248 ± 0.021	-1	-0.634 ± 0.051	-0.575 ± 0.032
4	$+1/2$	0.381 ± 0.027	$-1/2$	-0.282 ± 0.064	-0.359 ± 0.024
5	-1	-0.682 ± 0.027	$+1$	0.537 ± 0.064	0.594 ± 0.030
6	$+1$	0.764 ± 0.027	$+1$	0.545 ± 0.061	0.440 ± 0.024
7	$-1/2$	-0.349 ± 0.027	$-1/2$	-0.404 ± 0.065	-0.355 ± 0.024

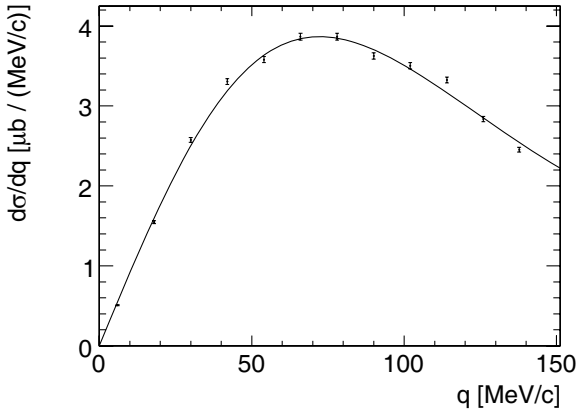

Fig. 12. Unpolarised differential cross-section for the $dp \to \{pp\}n$ reaction for $E_{pp} < 3\,\mathrm{MeV}$ compared with the impulse approximation predictions [11]. Only statistical errors are shown. There is in addition a global systematic uncertainty of about 6%.

change can induce high partial waves because of the large deuteron radius. This is to be contrasted with large momentum transfer deuteron break-up where the interaction is of much shorter range [23].

The variation of the cross-section with momentum transfer can be found in fig. 12 for $E_{pp} < 3\,\mathrm{MeV}$. The impulse approximation of sect. 2 also describes well the dependence on this variable out to $q = 140\,\mathrm{MeV}/c$. Once again it should be noted that no adjustment has been made to the model or the experimental data; the luminosity was evaluated independently using the quasi-free $np \to d\pi^0$ reaction.

6 Deuteron beam polarisation

The COSY polarised ion source that feeds the circulating beam was programmed to provide a sequence of one unpolarised state, followed by seven combinations of deuteron vector (P_z) and tensor (P_{zz}) polarisations, where z is the quantisation axis in the source frame of reference. The beam polarisation was measured in the COSY ring during the acceleration at a beam energy of $T_d = 270\,\mathrm{MeV}$ using the EDDA polarimeter [24]. The measurement of a variety of nuclear reactions in ANKE did not show any loss of beam polarisation when the deuterons were subsequently brought up to the experimental energy of $T_d = 1170\,\mathrm{MeV}$ [12].

Although the EDDA systematic uncertainties are quite low, as can be seen from table 1, only limited statistics were collected and this we alleviate by using the internal consistency of our deuteron charge-exchange data themselves. According to impulse approximation predictions [5,11], the deuteron vector analysing power for the $\vec{d}p \to \{pp\}n$ reaction should vanish for small excitation energies. Since the values of P_z can have no effect for $\theta_{pp} \approx 0$, this hypothesis can be tested by comparing the charge-exchange count rates, normalised on the BCT, for small and larger diproton angles. Any deviations from linearity could be ascribed to a it_{11}-dependence since table 1 shows that the eight modes have widely different values of P_z. All the data presented in fig. 13a fit well to a straight line, which reinforces the belief that the charge exchange is, as expected, only sensitive to the value of P_{zz}.

In fig. 13b the totality of the charge-exchange data is compared to the values of P_{zz} measured with the EDDA polarimeter. The scatter is larger due to the EDDA statistical errors but a linear fit is a good representation of the data. We then replace the EDDA values of P_{zz} for each of the individual modes by those corresponding to the linear regression shown in fig. 13b and these standardised values are given in table 1. This procedure retains the average dependence on the EDDA polarisations while reducing the statistical fluctuations inherent therein.

Although in the earlier work [12] the results were presented in terms of Cartesian analysing powers, the extrapolation to $q = 0$ is more stable when linear combinations corresponding to those in a spherical basis are used. The relation between the two is [25]

$$A_{yy} = -t_{20}/\sqrt{2} - \sqrt{3}\,t_{22}\,,$$
$$A_{xx} = -t_{20}/\sqrt{2} + \sqrt{3}\,t_{22}\,. \qquad (6.1)$$

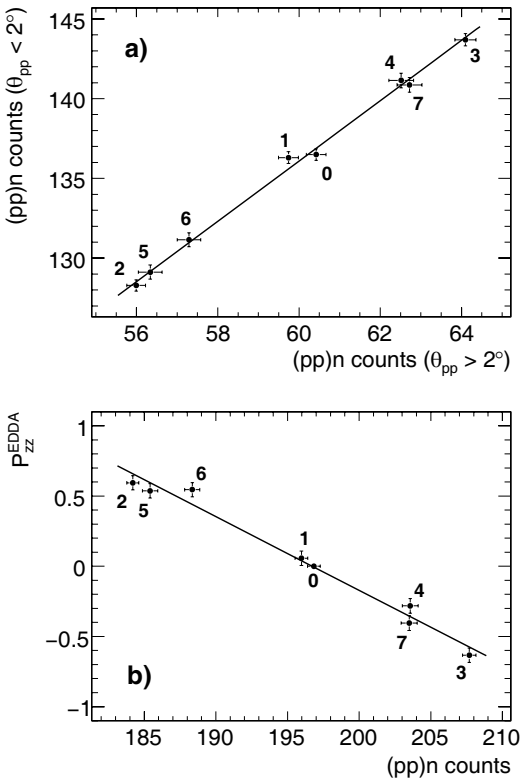

Fig. 13. Normalised counts $\times 10^{-3}$ for the $dp \to \{pp\}n$ reaction for the eight different source modes of table 1, (a) for events where the diproton laboratory angle is less than 2° compared to events where the angle is greater than 2°, and (b) compared to the EDDA measurements of the beam tensor polarisation [24]. Also shown are straight line fits to the data.

The differential cross-section for a polarised $\vec{d}p \to \{pp\}n$ reaction then becomes

$$\frac{\mathrm{d}\sigma}{\mathrm{d}t}(q,\phi)\Big/\left(\frac{\mathrm{d}\sigma}{\mathrm{d}t}(q)\right)_0 = 1 + \sqrt{3}P_z it_{11}(q)\cos\phi - \frac{1}{2\sqrt{2}}P_{zz}t_{20}(q) - \frac{\sqrt{3}}{2}P_{zz}t_{22}(q)\cos(2\phi), \qquad (6.2)$$

where the 0 subscript refers to the unpolarised cross-section. We are here using a right-handed coordinate system where the beam defines the z-direction and y is along the upward normal to the COSY orbit. The polar angle θ is measured with respect to the z-axis and the azimuthal angle ϕ with respect to the x.

7 Analysing powers of the deuteron charge-exchange reaction

Having identified the charge-exchange events, as described for the unpolarised case of sect. 5, the data were corrected for beam current and dead time and placed in 20 MeV/c bins in q and ten in $\cos 2\phi$. This procedure was carried out for two ranges in excitation energy, $0.1 < E_{pp} < 1$ MeV and $1 < E_{pp} < 3$ MeV. Although it is clear from fig. 10

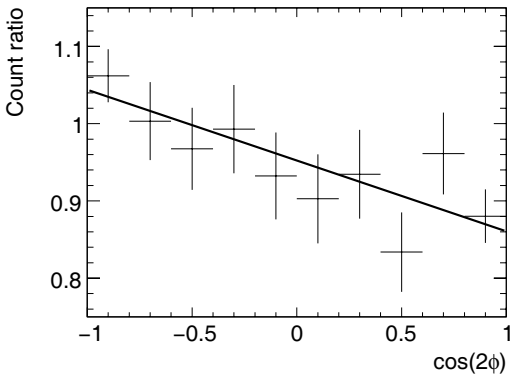

Fig. 14. Azimuthal angular dependence of the ratio of the normalised $dp \to \{pp\}n$ countrates for the source mode 5 to the average of modes 0 and 1, which have no tensor polarisation. Here the data are shown for the bin $40 < q < 60$ MeV/c and $E_{pp} < 1$ MeV. The linear fit in $\cos 2\phi$ allows the analysing power to be extracted by fitting the data to the right-hand side of eq. (6.2).

that the acceptance in terms of the azimuthal angle ϕ is well reproduced by the simulation, we have used modes 0 and 1, where there is zero tensor polarisation, to provide the best estimate of the denominator in eq. (6.2). By doing this we are using the fact that the geometric acceptances should be universal, *i.e.*, independent of the polarisation mode of the ion source. An example of the linear fit is shown in fig. 14 for polarisation mode 5.

The analysing powers of the $\vec{d}p \to \{pp\}n$ reaction were subsequently evaluated by fitting with eq. (6.2) and using the beam polarisations of modes 2 to 7 quoted in table 1. An estimate of the statistical errors inherent in this procedure could be obtained by studying the scatter of the results for these six polarisation modes of the source. A similar procedure in terms of $\cos\phi$ allowed bounds to be obtained on the vector analysing power but, as expected from both theory and the linearity of fig. 13a, all the data are consistent with it_{11} vanishing within error bars. The averages over the whole q range are $\langle it_{11}\rangle = -0.001 \pm 0.004$ for $E_{pp} < 1$ MeV and -0.004 ± 0.004 for $1 < E_{pp} < 3$ MeV.

Our experimental values of the two tensor analysing powers are shown in fig. 15 for the two ranges in E_{pp} as a function of the momentum transfer. The signals both fall when E_{pp} rises due to the influence of higher partial waves. This dilution can be partially offset by making a cut on the angle between $\boldsymbol{q}$ and $\boldsymbol{k}$ since P-waves are not excited when $\boldsymbol{q} \cdot \boldsymbol{k} = 0$ [5]. Therefore the data with small values of $|\cos\theta_{qk}|$ are far less affected by the E_{pp} cut.

The rapid rise of t_{22} with q is mainly a result of the fall in the $\delta(q)$ amplitude which, in a simple absorbed one-pion-exchange model, should vanish for $q \approx m_\pi c$. The behaviour can therefore be understood semi-quantitatively on the basis of eq. (2.9). The much smoother variation of t_{20} is also expected, with a gentle decline from the forward value, once again being mainly driven by the fall in the $\delta(q)$ amplitude. All these features are well reproduced by the impulse approximation model [11] using reliable np amplitudes [1].

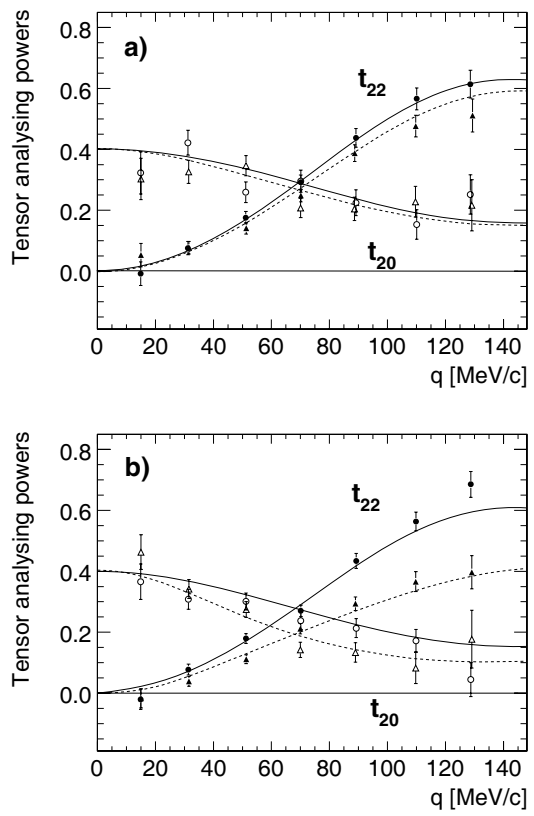

Fig. 15. Spherical tensor analysing powers t_{20} (open symbols) and t_{22} (closed symbols) for the $dp \to \{pp\}n$ reaction at $T_d = 1170\,\mathrm{MeV}$ for (a) $0.1 < E_{pp} < 1.0\,\mathrm{MeV}$ and (b) $1.0 < E_{pp} < 3.0\,\mathrm{MeV}$. The circles correspond to data where $|\cos\theta_{qk}| < 0.5$ while the triangles denote the results for $|\cos\theta_{qk}| > 0.5$. The solid and dashed curves are the impulse approximation predictions [11] for the same angular selections, respectively.

Although all the experimental data agree with the impulse approximation model one could, of course, invert the question. How well could one determine the amplitudes if there were no information available from the np phase shifts? Although the data reported here were obtained over only two-day run, these are already sufficient to determine quite well the ratio of the $|\varepsilon(0)|/|\beta(0)|$ in the forward direction. Since little dilution of the t_{20} signal is expected at $q = 0$, all the data for $E_{pp} < 3\,\mathrm{MeV}$ were fitted to a quadratic in q^2 for $q \le 100\,\mathrm{MeV}/c$. The value obtained at the origin gives $t_{20}(0) = 0.37 \pm 0.02$, where the error is purely statistical. The uncertainty introduced by the beam polarisation would, however, contribute less than ± 0.01 to this.

Since $\gamma(0) = 0$, $\delta(0) = \beta(0)$ and $\mathcal{R}(0) = 1$, the one surviving tensor analysing power of eq. (2.9) at $q = 0$ is given by

$$t_{20}(0) = \sqrt{2}\left(\frac{|\beta(0)|^2 - |\varepsilon(0)|^2}{2|\beta(0)|^2 + |\varepsilon(0)|^2}\right). \qquad (7.1)$$

Given that the P-waves have negligible effect at $q = 0$, this result translates into an amplitude ratio of

$$|\varepsilon(0)|/|\beta(0)| = 0.61 \pm 0.03. \qquad (7.2)$$

This is to be compared to the SAID value of 0.58, though no error can be deduced directly on their prediction [1]. The precision here is, of course, better than that which is achieved for the absolute value of the forward amplitudes, where the overall normalisation and other effects introduce another 3% uncertainty.

8 Conclusions

The deuteron has often been successfully used as a substitute for a free neutron target, especially for the measurement of spin observables [26]. In this pilot study we have shown that the measurements of the differential cross-section and two deuteron tensor analysing powers of the $\vec{d}p \to \{pp\}n$ reaction at 585 MeV per nucleon agree very well with the predictions based upon modern phase shift analyses [1]. There is no obvious reason why this success should not be repeated at higher energies where the neutron-proton database has far more ambiguities. They should then allow one to deduce values of the magnitudes of the amplitudes $|\beta(q)|^2 + |\gamma(q)|^2$, $|\delta(q)|^2$, and $|\varepsilon(q)|^2$.

In addition to extending the ANKE measurements to the maximum COSY energy of 1.15 GeV per nucleon, experiments are being undertaken with polarised beam and target [27]. The values of the two vector spin-correlation parameters depend upon the interferences of ε with the β and δ amplitudes [28]. Furthermore, the use of inverse kinematics with a polarised proton incident on a polarised deuterium gas cell [9] will allow the study to be continued up to 2.9 GeV per nucleon [8]. In future experiments an independent check on the luminosity will be provided through the study of the energy loss of the circulating beam in COSY [29].

On the other hand the low excitation energy charge exchange on the deuteron gives no direct information on the spin-independent amplitude α, whose magnitude can only be estimated by comparing the deuteron data with the free $np \to pn$ differential cross-section. It is seen, for example, from eq. (2.10), that the value of $|\alpha(0)|^2$ can be determined with respect to the other amplitudes by measuring the ratio of the charge exchange on the deuteron and proton [3].

At $q = 0$ there is potential redundancy between the measurement of the $dp \to \{pp\}n$ and $np \to pn$ cross-sections, though the normalisation is much easier to achieve with a beam of charged particles. Using this information in association with data on total cross-section differences, it seems likely that a clear picture of the neutron-proton charge-exchange amplitudes in the forward direction will emerge [2].

We are grateful to R. Gebel, B. Lorentz, H. Rohdjeß, and D. Prasuhn and other members of the accelerator crew for the

reliable operation of COSY and the deuteron polarimeters. We would like to thank I.I. Strakovsky for providing us with up-to-date neutron-proton amplitudes. We have also profited from discussions with F. Lehar. This work has been supported by the COSY FFE program, HGF-VIQCD, and the Georgian National Science Foundation Grant (GNSF/ST06/4-108).

References

1. R.A. Arndt, I.I. Strakovsky, R.L. Workman, Phys. Rev. C **62**, 034005 (2000); `http://gwdac.phys.gwu.edu`.
2. F. Lehar, C. Wilkin, Eur. Phys. J. A **37**, 143 (2008).
3. N.W. Dean, Phys. Rev. D **5**, 1661; 2832 (1972).
4. V.I. Sharov *et al.*, Czech. J. Phys. **56**, F117 (2006); Dubna preprint E1-2008-61 (2008).
5. D.V. Bugg, C. Wilkin, Nucl. Phys. A **467**, 575 (1987).
6. C. Ellegaard *et al.*, Phys. Rev. Lett. **59**, 974 (1987).
7. S. Kox *et al.*, Nucl. Phys. A **556**, 621 (1993).
8. A. Kacharava, F. Rathmann, C. Wilkin, *Spin Physics from COSY to FAIR*, COSY proposal **152** (2005) arXiv:nucl-ex/0511028.
9. K. Grigoryev *et al.*, AIP Conf. Proc. **915**, 979 (2007).
10. D. Chiladze *et al.*, Phys. Lett. B **637**, 170 (2006).
11. J. Carbonell, M.B. Barbaro, C. Wilkin, Nucl. Phys. A **529**, 653 (1991).
12. D. Chiladze *et al.*, Phys. Rev. ST Accel. Beams **9**, 050101 (2006).
13. R. Maier *et al.*, Nucl. Instrum. Methods A **390**, 1 (1997).
14. S. Barsov *et al.*, Nucl. Instrum. Methods A **462**, 364 (2001).
15. S. Dymov *et al.*, Part. Nucl. Lett. **1**, 40 (2004).
16. A. Khoukaz *et al.*, Eur. Phys. J. D **5**, 275 (1999).
17. Pluto WEB page: `http://www-hades.gsi.de/computing/pluto/html/PlutoIndex.html`.
18. M. Lacombe *et al.*, Phys. Lett. B **101**, 139 (1981).
19. R.A. Arndt, I.I. Strakovsky, R.L. Workman, D.V. Bugg, Phys. Rev. C **48**, 1926 (1993); `http://gwdac.phys.gwu.edu/analysis/pd_analysis.html/`.
20. E.T. Boschitz *et al.*, Phys. Rev. C **6**, 457 (1972).
21. N. Katayama, F. Sai, T. Tsuboyama, S.S. Yamamoto, Nucl. Phys. A **438**, 685 (1985).
22. R.J. Glauber, in *Lectures in Theoretical Physics*, edited by W.E. Brittin, Vol. **1** (Interscience, New York, 1959) p. 315.
23. V.I. Komarov *et al.*, Phys. Lett. B **553**, 179 (2003).
24. B. Lorentz *et al.*, in *Proceedings of the 9th European Particle Accelerator Conference, Lucerne, Switzerland, 2004* (EPS-AG CERN, Geneva, 2005) p. 1246.
25. G.G. Ohlsen, Rep. Prog. Phys. **35**, 717 (1972).
26. A. de Lesquen *et al.*, Eur. Phys. J. C **11**, 69 (1999).
27. R. Engels *et al.*, AIP Conf. Proc. **980**, 161 (2007).
28. M.B. Barbaro, C. Wilkin, J. Phys. G **15**, L69 (1989).
29. H.J. Stein *et al.*, Phys. Rev. ST Accel. Beams **11**, 052801 (2008).